Photoluminescence quantum yields of amorphous and crystalline silicon nanoparticles

Rebecca Anthony and Uwe Kortshagen
Department of Mechanical Engineering, University of Minnesota, 111 Church Street Southeast, Minneapolis, Minnesota 55455, USA
(Received 23 February 2009; revised manuscript received 23 July 2009; published 9 September 2009)

While nanocrystalline silicon is known to be an efficient optical emitter, there have been few and sometimes contradictory reports of emission from amorphous silicon nanoparticles. This paper presents a study of the optical properties of amorphous and crystalline silicon nanoparticles synthesized by a nonthermal plasma reactor. By tuning the power delivered to the reactor, the particle structure was adjusted from amorphous to crystalline without otherwise changing the particle properties, such as nanoparticle size, in a significant manner. Two different kinds of surface passivation of nanoparticles are studied: the surface functionalization with organic ligands in a scheme known as hydrosilylation and the passivation with a native surface oxide. We observe a clear trend of the photoluminescence quantum yield increasing with the increasing degree of crystallinity of samples with largely amorphous samples, exhibiting almost no luminescence. Measurements suggest that the upper bound for the quantum yield of amorphous nanoparticles is 2%, while the quantum yield of silicon nanocrystals is routinely found to exceed 40%.

DOI: 10.1103/PhysRevB.80.115407 PACS number(s): 78.67.Bf, 78.30.Am

I. INTRODUCTION

Since the first observation of efficient photoluminescence (PL) from nanoscale silicon,[1,2] this topic has attracted considerable attention due to the potentially high PL efficiencies that can be achieved over a broad spectral range from silicon nanocrystals (NCs). As an indirect band-gap semiconductor, bulk silicon is an inefficient optical emitter and absorber. However, it is now widely accepted that the optical properties of nanoscale crystalline silicon are considerably improved due to a combination of two effects: the enhanced overlap of electron and hole wave functions in quantum-confined silicon leading to faster recombination[3] and the reduction in the rate of nonradiative events.[4]

There have been a number of reports that have demonstrated that nanocrystalline silicon can achieve photoluminescence quantum yields rivaling those of direct band-gap semiconductors. An important measure of the optical quality of silicon nanocrystals is the quantum yield (QY) for photoluminescence defined as the number of photons emitted divided by the number of exciting photons absorbed. While silicon nanocrystals passivated by native oxide layers typically have PL QYs of up to about 10%, there have been limited reports of even higher quantum yields of up to 30%.[5] High QYs were also found for the silicon nanocrystals embedded in high-quality thermal oxides.[6] The surface functionalization with organic monolayers is another proven way to achieve high-efficiency PL from silicon nanocrystals.[7,8] In Refs. 9 and 10, we reported QYs as high as 70% for ensembles of nonthermal plasma produced silicon nanocrystals[11] whose surfaces were treated with 1-dodecene under careful avoidance of oxygen. Moreover, in single-quantum dot experiments, PL QYs as high as 88% were observed for individual quantum dots.[12] However, these studies also found an often large difference between the QYs of individual particles and nanocrystal ensembles, whose QYs were found to be on the order of just a few percent due to the large fraction of "dark," i.e., nonemitting, particles.

Significantly fewer reports have addressed optical emissions from amorphous silicon nanoclusters. Several groups[13–17] have reported photoluminescence from amorphous silicon nanoparticles embedded in solid-state matrices. In the work by Park *et al.*,[16,17] several sizes of amorphous silicon nanoparticles were produced in SiO_2. Size-tunable photoluminescence from these amorphous particles was reported ranging from blue to red. The blueshift of photoluminescence energy upon shrinkage of particle size indicated that quantum confinement effects may be seen in amorphous nanoscale silicon. In the paper by Molinari *et al.*,[18] it was suggested that the PL from amorphous silicon nanoclusters in SiO_2 and Si_3N_4 matrices is due to quantum confinement but that the emission intensity and efficiency are lower than those for nanocrystalline particles because of the higher number of nonradiative recombination centers in amorphous clusters. This group proposes that well-passivated crystalline silicon nanoparticles will have much more intense PL due to fewer of these defects. Work presented in Refs. 19 and 20 arrives at similar conclusions. While luminescence could be observed from amorphous nanoparticles (a-NPs), the luminescence from crystalline particles was found to be more efficient.

Previous studies of the emission of amorphous silicon nanoparticles have been limited to clusters embedded in dielectric matrices such as SiO_2 and Si_3N_4. In such systems, it is often difficult to distinguish between intrinsic limitations of the material itself and extrinsic limitations caused by the presence of the interface with the surrounding matrix. It is also difficult to perform absolute measurements of the photoluminescence quantum yield. In fact, such measurements have not been reported to date; hence, it is difficult to quantify what the reports of "efficient luminescence" from amorphous nanoparticles actually mean.

In this paper, we will study the PL efficiency of free-standing silicon a-NPs compared to those of free-standing silicon NCs. The use of free-standing nanoparticles suspended in colloidal solution enables the absolute measurement of the photoluminescence quantum yield, which is routinely reported in the nanocrystal literature, and which we had previously established for silicon nanocrystals.[9,10] Measurements of the absolute QY will enable us to quantify the

luminescence efficiency of amorphous silicon particles. The use of free-standing silicon particles also enables the same careful passivation of the amorphous nanoparticle surfaces that provided ensemble QYs as high as 70% for silicon nanocrystals[9,10] and may allow conclusions about the intrinsic luminescent potential of amorphous silicon nanoclusters.

The particle structure is varied between amorphous and crystalline by adjusting the power delivered to the plasma. We study silicon particles with surfaces functionalized both with organic monolayers and a native oxide layer. Results of absolute QY measurements for ensembles of amorphous and crystalline free-standing silicon nanoparticles are reported.

II. EXPERIMENTAL

We synthesized silicon nanoparticles in a nonthermal low-pressure plasma reactor, as described previously.[11] The quartz reactor has a 10-mm-outer diameter reaction area, where the radiofrequency electrode is placed, which then expands to 25-mm-outer diameter before exiting to the collection filter and pump. The size of the particles is controlled by adjusting the flow rate of argon gas through the reactor tube between 25 and 100 sccm (standard cubic centimeters per minute). Silane gas (5% in helium) was flown at 13.8 sccm and hydrogen gas was injected at 100 sccm in the 25 mm expansion region of the reactor tube. When the argon flow rate was greater than 50 sccm, 2 sccm of additional hydrogen was added to the reactant gas mixture. To change the crystallinity of the particles, we adjust the 13.56 MHz radiofrequency input power to the reactor between 25 and 100 W. Crystalline and amorphous particles of four sizes were synthesized from 3 to 5 nm in diameter. Following synthesis, some of the amorphous and crystalline particle samples of several sizes were surface processed with a 5:1 mixture of mesitylene and 1-dodecene in a liquid-phase thermal hydrosilylation reaction[10] to render them stable in nonpolar solvent dispersions and to help protect the nanoparticles from oxidation. For a sample of 5 nm NCs, the hydrosilylation procedure yields a clear colloidal dispersion of particles by the end of a 2 to 3 h refluxing period at 205–215 °C. This reaction time is fairly consistent for NCs. Reaction time increases with decreasing particle size, but even the smallest NCs examined in this study reacted with the 1-dodecene to form a clear colloid. While, due to steric hindrance of the ligand molecules, it is not expected that more than 30% to 40% of the silicon NC surface sites are functionalized with ligand molecules,[21] we showed in Ref. 22 that this procedure yields colloids of individually dispersed Si NCs. We also found that the remaining surface sites are covered with hydrogen from the plasma reaction. In this study we found that a-NPs require longer reaction times before a clear solution is obtained. In fact, for the smallest a-NPs, a clear colloidal dispersion is never achieved. This hints at a different surface structure of the a-NPs compared to NCs, which was not further examined in the present study.

To examine the effects of oxidation on the particle photoluminescence, several samples of each phase were dispersed while still bare (unfunctionalized) and were allowed to oxidize naturally due to contact with air in the environment. The PL from these samples was measured periodically. The particle samples were characterized in the University of Minnesota Materials Characterization Facility, using an FEI Tecnai T-12 transmission electron microscope (TEM) for TEM images, a Bruker-AXS Microdiffractometer for x-ray diffraction (XRD) spectra, and a confocal Raman microscope (Witec alpha300 R confocal Raman microscope with UHTS300 spectrometer and DV401 charge-coupled device) for Raman vibrational spectroscopy. The photoluminescence quantum yield of the nanoparticles was measured at room temperature using a light-emitting diode (LED) excitation source at 390–400 nm, an integrating sphere, and a USB2000 spectrometer (Ocean Optics, Inc.). The procedure for measuring quantum yields is described in detail in Ref. 10.

III. RESULTS

A. Nanoparticle structural characterization

An increase in plasma power generally leads to increasing crystallinity of the nanoparticle samples. In Ref. 23, we showed that nanoparticles immersed in a plasma get strongly heated to temperatures several hundreds of Kelvin beyond the gas temperature through exothermic surface reactions, including electron-ion recombination and hydrogen-induced surface reactions. An increase in plasma power leads to increasing densities of the species involved in these surface reactions including electrons, ions, and atomic hydrogen radicals. Hence, increasing the plasma power leads to a significant increase in the particle heating, which we expect to cause the transition from a-NPs to NCs with increasing power.

To verify the changing crystallinity of the nanoparticles, we synthesized several samples under the same flow and pressure parameters, with varying input powers. XRD patterns clearly show an increase in silicon particle crystallinity as we increase synthesis power (see Fig. 1).

We took Raman vibrational spectra to corroborate this conclusion and the emergence of a peak near 520 cm^{-1}, corresponding to crystalline silicon, demonstrates the increase in crystallinity with increasing power (see Fig. 2). It should be noted that a quantitative determination of the crystal fraction from Raman spectra is not straightforward, as the transverse optical peak near 520 cm^{-1} can be strongly asymmetric due the presence of strain and of a particle size distribution.[24] The XRD and Raman spectroscopy data shown here are consistent with the data found in the structural characterization of NCs by other authors.[25,26]

We also performed TEM studies to characterize both the size and microstructure of produced samples (see Fig. 3). The bright-field TEM images in Figs. 3(a) and 3(b) demonstrate that the produced particles are highly monodisperse. The a-NPs and NCs have approximately the same size. It is obvious that NCs have more well-defined spherical shapes, while the shapes of a-NPs are slightly more irregular. The selected-area electron-diffraction (SAED) pattern shows bright diffraction rings attributable to a polycrystalline sample in the high-power case [Fig. 3(b)], while the SAED pattern from the low-power sample shows only a diffuse

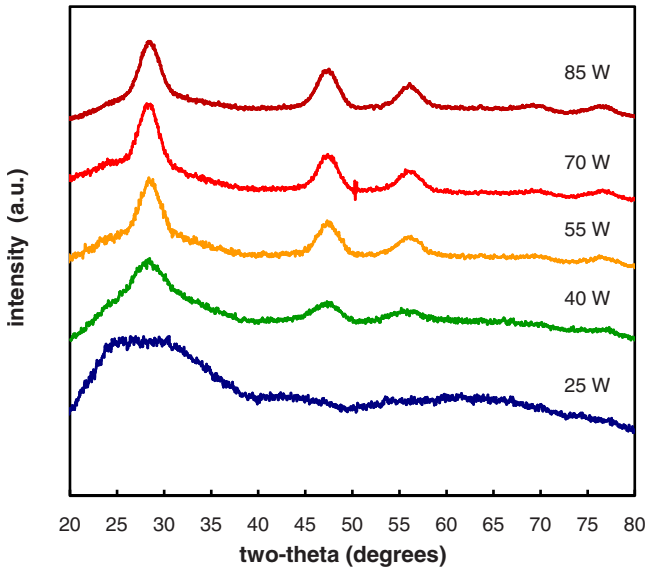

FIG. 1. (Color online) X-ray diffraction spectra for samples of varying synthesis powers. Peaks typical of silicon nanocrystallites are visible in all except the lowest-power sample.

glow, indicative of amorphous material [Fig. 3(a)]. Furthermore, well-defined bright areas of the dark-field image from the high-power sample further illustrate the crystallinity of the NCs [Fig. 3(d)]. In the low-power sample, the dark-field image shows no crystal definition [Fig. 3(c)].

B. Photoluminescence quantum yields

We recorded and analyzed the photoluminescence spectrum of each liquid sample of surface-functionalized silicon particles to obtain the sample's ensemble quantum yield.

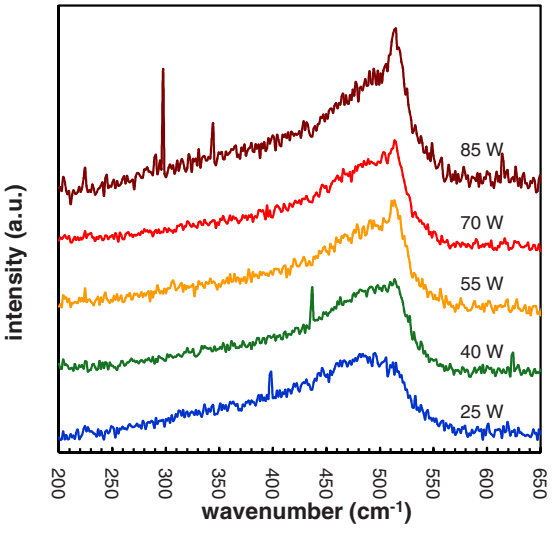

FIG. 2. (Color online) Raman spectra of silicon particle samples. The top spectrum is from a sample made at 85 W power, with synthesis power decreasing to 25 W as the spectra descend. The sharp peak near ~520 cm^{-1}, indicative of nanocrystallites, first appears for the 40 W sample, and becomes more prominent with increasing power.

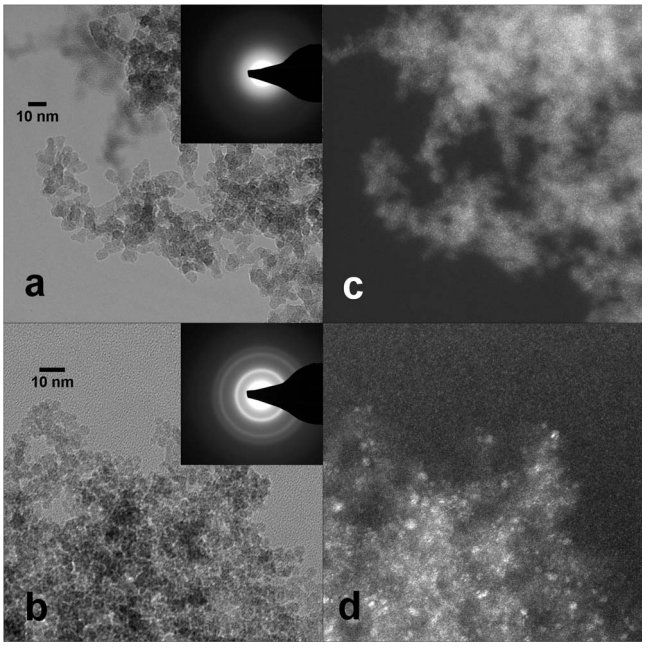

FIG. 3. Transmission electron images of silicon samples: (a) and (b) are bright-field images of a-NPs and NCs, respectively, with selected-area electron-diffraction patterns inset. (c) and (d) are dark-field images of a-NPs and NCs.

These measurements were taken with the NCs and a-NPs dispersed in the functionalizing mixture of 5:1 mesitylene:1-dodecene. With decreasing input power and, thus, decreasing particle crystallinity, the quantum yields decreased as well. In fact, the QYs from the samples of a-NPs were so low as to be hardly measurable using our instrument. Figure 4(a) displays a plot of PL QYs as a function of input power. All samples in this plot were synthesized with argon flow rates between 20–40 sccm. At high synthesis powers, high-efficiency photoluminescence of the NCs prevails; while at powers below 50 W, the samples do not exhibit the same high-efficiency photoluminescence. Samples generated with powers between 50–70 W show clear crystalline features in their XRD and Raman spectra. However, PL QYs for samples made at these powers vary from very low to moderately high, despite clear evidence that the samples have a measurable nanocrystalline fraction. The only samples for which we see consistently high-efficiency PL are those made

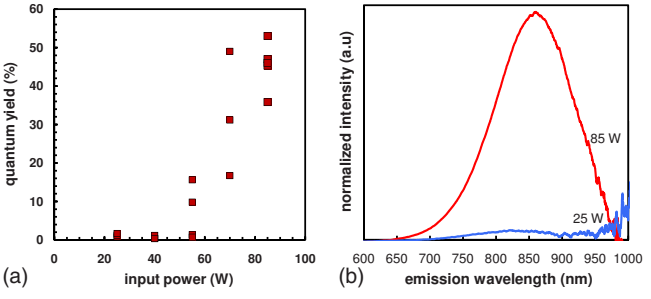

FIG. 4. (Color online) (a) Photoluminescence quantum yields of nanoparticle samples and (b) PL spectrum comparison between 85 and 25 W samples.

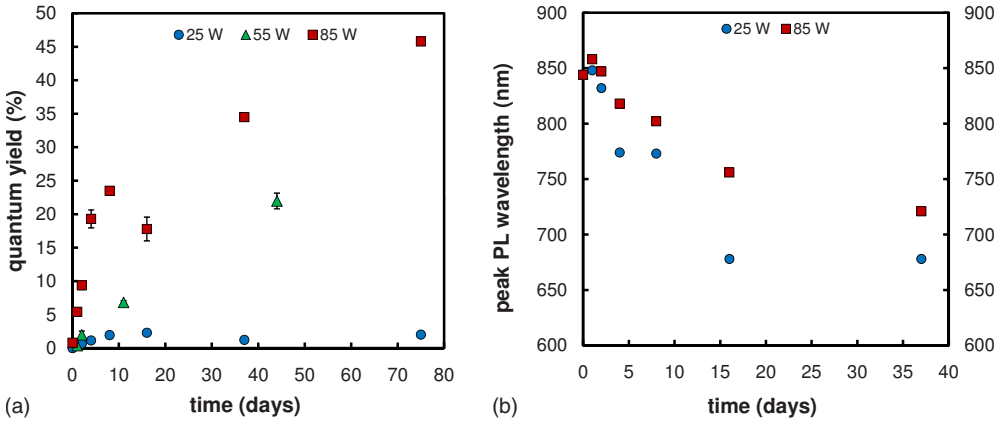

FIG. 5. (Color online) PL quantum yields of nanoparticle samples measured over time. The samples were unfunctionalized and allowed to oxidize, which acts to increase the quantum yields of crystalline samples (85 and 55 W) but has little pronounced effect on the amorphous sample. (a) Quantum yield; (b) peak PL wavelength.

at powers of 85 W or greater. A direct comparison of the photoluminescence spectra for NCs (85 W) and a-NPs (25 W) of the same size is shown in Fig. 4(b). The PL from the a-NP sample is clearly significantly weaker than PL from the NC sample. This behavior was consistently found for all sizes of the samples studied.

It is important to note that the system variability contributes significantly to the degree of sample-to-sample variability seen in Fig. 4(a). Each sample preparation requires partial disassembly and reassembly of the plasma reactor, which may cause slight changes in electrode position and other minor adjustments. We found that these lead to changes in the plasma conditions between samples which at the transition from the a-NP to the NC regime can lead to changes in the crystallinity for samples prepared at the same power. This likely explains why samples produced at 40 W show only very low quantum yield, yet the 40 W sample prepared for Raman (Fig. 2) and XRD (Fig. 1) diagnostic showed slight signatures for crystallinity. It likely also explains the strong sample-to-sample variation for the higher-power samples.

It is difficult to determine precisely whether the weak emission observed from low-power samples is indeed due to emission from a-NPs or caused by a very small and hard to detect fraction of NCs. For instance, if a-NPs were nonemitting, a fraction of 1% of nanocrystals with an intrinsic QY of 45% would be interpreted as a sample with an ensemble quantum yield of 0.45%, a value which is consistent with the values observed in our measurements [see Fig. 4(a)]. A crystalline fraction of a few percent in an otherwise amorphous sample would be difficult to detect with XRD or Raman scattering. However, the emission spectra in Fig. 4(b) suggest that the emission observed from the low-power sample may indeed originate from a small fraction of NCs in an otherwise amorphous sample. The emission of the a-NP sample produced at 25 W occurs at roughly the same emission wavelength as the emission of the NC sample produced at 85 W. While TEM observations suggest that the particle sizes for both samples are the same, the emission of silicon NCs and a-NPs is not necessarily expected to occur at the same wavelengths. As suggested by Park *et al.*,[16] the emission energy of quantum-confined amorphous silicon nanoclusters is expected to follow the relation:

$$E(\mathrm{eV}) = 1.56 + 2.4/a^2, \tag{1}$$

with a as the nanoparticle diameter. Hence, even for large a-NPs, emission should not be expected at wavelengths larger than ~790 nm (i.e., 1.56 eV). However, it is clearly observed from the a-NP sample in Fig. 4(b). This suggests that the emission observed from the a-NP sample is from a small fraction of NCs that is too small to be observed with XRD or Raman.

While the classification of samples as "amorphous" is obviously not entirely unambiguous, the measurements presented here allow us to place an upper bound on the absolute QY of a-NPs in that no sample that we characterized as amorphous has shown a QY larger 2%. Hence, we can establish 2% as the upper bound for the absolute QY of freestanding silicon a-NPs with hydrosilylated surfaces, which is considerably lower than the QYs of ~50% observed for NCs with the same surface treatment.

C. Oxidation experiments

Hydrosilylation is one mechanism of passivating dangling bonds at the nanoparticle surface[27] through the organic ligands and surface hydrogen and, thus, increasing ensemble quantum yields of the NCs, while a-NPs show PL with very low QY. However, many of the reports of PL from silicon a-NPs were based on particles embedded in a matrix of silicon nitride or silicon dioxide. To emulate these conditions, we allowed some samples to oxidize in order to study the PL of particles when coated in an oxide shell. The formation of a native oxide shell on silicon nanocrystals is known to lead to an increase in the PL QY since the native oxide removes nonradiative surface states.[5]

We synthesized samples at 25, 55, and 85 W then dispersed the samples in chloroform and allowed them to oxidize via exposing the samples to air. As time progressed, we measured the quantum yields of these samples periodically [see Fig. 5(a)].

The samples made at 85 W initially had low PL efficiency, which increased in time as the particles oxidized. The growth of the oxide layer passivates the surface defects, leaving the NC core intact and able to emit efficiently. The samples also

showed a blueshift in emission energy, in accordance with a shrinking nanocrystalline core [Fig. 5(b)], as the quantum-confined exciton energy is size dependent.[28] While the rate of emission blueshift was rapid in the early stages of oxidation, over a period of several months, this rate slowed to near zero. This blueshift was present in all samples prepared at different power levels. The sample prepared at 55 W shows a lower QY than the sample at 85 W, consistent with the likely lower crystalline fraction of this sample.

The 25 W sample characterized as amorphous consistently displayed low QY despite experiencing the same oxidation conditions as the 85 W sample. Hence, the free-standing a-NPs, even after surface oxidation do not exhibit high-efficiency PL as was reported in other work.[15,29] Again, it is not possible to determine whether the weak PL of this sample originates from the oxidized a-NPs or from a very small fraction of NCs that remain undetectable by Raman scattering and XRD. However, the fact that the luminescence spectrum shows comparable blueshift of the peak PL as the highly crystalline 85 W sample suggests that emission in fact originates from a small fraction of NCs in the 25W sample. As above, while this measurement is not entirely unambiguous, we can use it to define an upper bound for the absolute PL QY of oxidized a-NPs of about 2%. This is significantly less efficient than the QY of oxidized Si NCs, which ranges as high as ~45%—a number consistent with observations in earlier studies.[5]

It is likely that the properties of the oxide used in Refs. 15 and 29 are different from the native oxide formed at room temperature in our work. Hence, it is difficult to draw direct comparisons to those studies. However, for the free-standing silicon a-NPs produced in this work high-efficiency PL was not observed. The upper bound for the absolute PL QY was found to be ~2% regardless of surface functionalization.

IV. CONCLUSIONS

In this paper, we studied the photoluminescence efficiency of free-standing silicon NCs and a-NPs. The crystallinity of silicon nanoparticles made in a nonthermal plasma reactor may be tuned simply by adjusting the input synthesis power. For our specific experimental setup, at powers greater than 55 W, samples with high crystallinity are obtained, whereas powers lower than 55 W yield primarily a-NPs. The surfaces of Si NCs and a-NPs were treated with two different surface functionalizations: the assembly of organic alkene monolayers through hydrosilylation and the coating of the surfaces through native oxide formation. Regardless of surface functionalization, the a-NPs synthesized in the plasma reactor do not exhibit high-efficiency photoluminescence, while NCs produced routinely exhibit PL QYs greater than 40%. All a-NP samples showed PL QY $<2\%$. This result defines an upper bound for the absolute QY of the free-standing silicon a-NPs studied in this work. However, as the a-NP PL was found to be much weaker but similar in wavelength and temporal evolution to that of the silicon NC samples, we suggest that the a-NP sample PL in fact originates from a small fraction of NCs that is not detected by XRD or Raman scattering. This would imply that the intrinsic absolute QY of silicon a-NPs is in fact even smaller than the 2% defined as upper bound.

ACKNOWLEDGMENTS

This research was primarily supported by the NSF under MRSEC Grant No. DMR-0819885. Partial support by the NSF IGERT Grant No. DGE-0114372 is acknowledged. Parts of this work were carried out in the Institute of Technology Materials Characterization Facility, University of Minnesota, which receives partial support from the NSF through the NNIN program.

[1] L. T. Canham, Appl. Phys. Lett. **57**, 1046 (1990).
[2] A. G. Cullis and L. T. Canham, Nature (London) **353**, 335 (1991).
[3] C. Delerue, G. Allan, and M. Lannoo, Phys. Rev. B **64**, 193402 (2001).
[4] L. E. Brus, P. J. Szajowski, W. L. Wilson, T. D. Harris, S. Schuppler, and P. H. Citrin, J. Am. Chem. Soc. **117**, 2915 (1995).
[5] G. Ledoux, J. Gong, F. Huisken, O. Guillois, and C. Reynaud, Appl. Phys. Lett. **80**, 4834 (2002).
[6] R. J. Walters, J. Kalkman, A. Polman, H. A. Atwater, and M. J. A. de Dood, Phys. Rev. B **73**, 132302 (2006).
[7] J. D. Holmes, K. J. Ziegler, C. Doty, L. E. Pell, K. P. Johnston, and B. A. Korgel, J. Am. Chem. Soc. **123**, 3743 (2001).
[8] R. M. Sankaran, D. Holunga, R. C. Flagan, and K. P. Giapis, Nano Lett. **5**, 537 (2005).
[9] D. Jurbergs, L. Mangolini, E. Rogojina, and U. Kortshagen, Appl. Phys. Lett. **88**, 233116 (2006).
[10] L. Mangolini, D. Jurbergs, E. Rogojina, and U. Kortshagen, J. Lumin. **121**, 327 (2006).
[11] L. Mangolini, E. Thimsen, and U. Kortshagen, Nano Lett. **5**, 655 (2005).
[12] G. M. Credo, M. D. Mason, and S. K. Buratto, Appl. Phys. Lett. **74**, 1978 (1999).
[13] W. Yu, J. Y. Zhang, W. G. Ding, and G. S. Fu, Eur. Phys. J. B **57**, 53 (2007).
[14] Y. Q. Wang, W. D. Chen, X. B. Liao, and Z. X. Cao, Nanotechnology **14**, 1235 (2003).
[15] X. D. Pi, O. H. Y. Zalloum, T. Roschuk, J. Wojcik, A. P. Knights, P. Mascher, and P. J. Simpson, Appl. Phys. Lett. **88**, 103111 (2006).
[16] N.-M. Park, C.-J. Choi, T.-Y. Seong, and S.-J. Park, Phys. Rev. Lett. **86**, 1355 (2001).
[17] N.-M. Park, T.-S. Kim, and S.-J. Park, Appl. Phys. Lett. **78**, 2575 (2001).
[18] M. Molinari, H. Rinnert, and M. Vergnat, Europhys. Lett. **66**, 674 (2004).
[19] A. Irrera *et al.*, Nanotechnology **17**, 1428 (2006).
[20] S. Boninelli, F. Iacona, G. Franzò, C. Bongiorno, C. Spinella, and F. Priolo, J. Phys.: Condens. Matter **19**, 225003 (2007).
[21] X.-Y. Zhu, V. Boiadjiev, J. Mulder, R. Hsung, and R. Major,

Langmuir **16**, 6766 (2000).
[22] L. Mangolini, D. Jurbergs, E. Rogojina, and U. Kortshagen, Phys. Status Solidi C **3**, 3975 (2006).
[23] L. Mangolini and U. Kortshagen, Phys. Rev. E **79**, 026405 (2009).
[24] V. Tripathi, M. N. Islam, Y. Mohapatra, and P. R. i. Cabarrocas, Eur. Phys. J. Appl. Phys. **39**, 203 (2007).
[25] A. A. Sirenko, J. R. Fox, I. A. Akimov, X. X. Xi, S. Ruminov, and Z. Liliental-Weber, Solid State Commun. **113**, 553 (2000).
[26] V. Kapaklis, C. Politis, P. Poulopoulos, and P. Schwiess, Appl. Phys. Lett. **87**, 123114 (2005).
[27] J. Buriak, Chem. Rev. **102**, 1271 (2002).
[28] A. Zunger and L. W. Wang, Appl. Surf. Sci. **102**, 350 (1996).
[29] H. Rinnert, M. Vergnat, G. Marchal, and A. Burneau, Appl. Phys. Lett. **72**, 3157 (1998).